Rapid Communications

Light-induced new collective modes in the superconductor $La_{1.905}Ba_{0.095}CuO_4$

S. J. Zhang,[1] Z. X. Wang,[1] L. Y. Shi,[1] T. Lin,[1] M. Y. Zhang,[1] G. D. Gu,[2] T. Dong,[1,*] and N. L. Wang[1,3,†]

[1]*International Center for Quantum Materials, School of Physics, Peking University, Beijing 100871, China*

[2]*Condensed Matter Physics and Materials Science Department, Brookhaven National Lab, Upton, New York 11973, USA*

[3]*Collaborative Innovation Center of Quantum Matter, Beijing 100871, China*

(Received 4 December 2017; revised manuscript received 11 July 2018; published 24 July 2018)

We report near and midinfrared pump, c-axis terahertz probe measurements on a superconducting single crystal $La_{1.905}Ba_{0.095}CuO_4$ with $T_c = 32$ K. The measurements reveal that the pump-induced change occurs predominantly at the Josephson plasma edge position below T_c. Upon excitation by strong near-infrared pulses, the superconducting state is severely disturbed and incoherent quasiparticle excitations develop in the frequency regime above the static plasma edge. However, within a very short time delay (∼1.5 ps) we observe the reappearance of a very sharp Josephson plasma edge at a frequency lower than the static Josephson plasma edge and the emergence of a new light-induced edge at a higher energy. The results imply that the light can induce new Josephson plasmon modes with different coupling strengths. A similar but weaker effect is observed for the midinfrared pump. No pump-induced effect is detected above T_c.

DOI: 10.1103/PhysRevB.98.020506

The recent development of ultrashort laser pulses has been proven to be a powerful tool for the light control of different orders in complex electronic materials. Paradigmatic examples include the induction of lattice distortions in manganites [1], the transient generation of spin-density-wave order in the normal state of $BaFe_2As_2$ [2], melting [3] and switching [4] of charge-density-wave (CDW) orders in transition-metal dichalcogenides, manipulation of the order parameters and detection of Higgs/amplitude modes in superconductor/CDW compounds [5,6], light-induced electron localization in a quantum Hall system [7], etc. Among various novel phenomena, the light-induced superconductivity in cuprates is perhaps the most intriguing observation. The effect was first observed in a stripe-ordered cuprate at 10 K in the normal state [8], then in underdoped $YBa_2Cu_3O_{6.5}$ at temperatures even above 300 K [9,10]. In those measurements, after being excited by midinfrared (MIR) 15 μm (∼80 meV), the Josephson plasma edges formed by superfluid carriers were detected in a time-domain terahertz (THz) measurement. More recently, it was found that the transient superconductivity could be induced and enhanced by a near-infrared (NIR) pump at 800 nm (∼1.55 eV) in $La_{1-x}Ba_xCuO_4$ with $x = 0.115$, which is close to the stripe-ordered phase [11,12].

Here, we report a photoexcited c-axis dynamics in a superconducting single crystal $La_{1.905}Ba_{0.095}CuO_4$ with $T_c = 32$ K [13], by using NIR (1.28 μm, ∼ 1 eV) and MIR (15 μm) pump and THz probe measurements. We find that strong NIR pumping suppresses the superconductivity and induces incoherent quasiparticle excitations. However, within a very short time delay, ∼1.5 ps, we observe the reappearance of a very sharp Josephson plasma edge at an energy lower than the static Josephson plasma edge and the emergence of a new light-induced edge at a higher energy. The results suggest the establishment of new Josephson plasmon modes from condensed superfluid carriers with different coupling strengths. A weaker effect is found for the MIR pumping. The result is very different from an earlier report by Nicoletti *et al.* on the same composition, in which they found a negligibly small effect with an 800-nm pump at a fluence of 2 mJ/cm^2 [11].

A near to midinfrared pump–THz probe spectroscopy system was constructed to measure the c-axis static and pump-induced time-domain THz electric field [14]. A transverse electric field (TE) configuration, i.e., the THz electric field being perpendicular to the incident plane, is employed for the measurement, as displayed in Fig. 1(a). Details of the experimental setup and measurement technique are presented in the Supplemental Material [15]. Figure 1(b) shows the far-infrared (FIR) reflectivity spectra with the electric field of the light $E \parallel c$ axis at two selective temperatures measured by a Fourier transform infrared spectrometer (FTIR). The spectra show a number of phonon modes in the FIR region. Above T_c, the reflectivity values are low and relatively featureless below 100 cm^{-1} (or 3 THz), indicating an insulating response. Below T_c, a very sharp Josephson plasma edge develops near 18 cm^{-1} (∼0.54 THz) at 6 K. The data are in good agreement with the earlier measurement by Homes [16]. Figures 1(c) and 1(d) show static THz spectra in the time domain $E(t)$ and their Fourier-transformed spectra in the frequency domain $E(\omega)$ at two selective temperatures 35 and 6 K above and below T_c, respectively. The sharp dip near 18 cm^{-1} at 6 K corresponds to the Josephson plasma edge observed in the FTIR measurement. The presence of a Josephson plasmon is a hallmark of superconductivity in layered cuprates.

We now show the time-resolved terahertz measurement with a NIR pump at 1.28 μm. Figure 2(a) displays the decay of the relative change of the THz electric field peak $\Delta E/E_{\text{peak}}$ after excitation by a fluence of 3 mJ/cm^2. We define time zero

*taodong@pku.edu.cn
†nlwang@pku.edu.cn

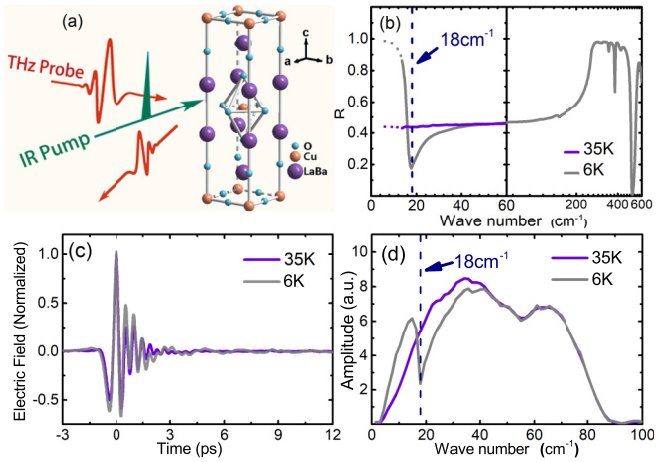

FIG. 1. Crystal structure and equilibrium optical spectra. (a) Both the pump and THz probe electric fields are polarized to the c axis of the sample. (b) The FIR reflectance spectra measured by FTIR at two selective temperatures 35 and 6 K above and below T_c, respectively. The reflectance extension to lower energy (dot curves) is achieved by the time-domain THz measurement. (c) and (d) Static THz spectra in the time domain $E(t)$ and their Fourier-transformed spectra in the frequency domain $E(\omega)$ at 35 and 6 K. The dashed line indicates the plasma edge dip position.

$\tau = 0$ ps at the maximum position of the pump-probe signal $\Delta E/E_{\text{peak}}$, and the "static" state before where $\Delta E/E_{\text{peak}}$ starts to change. A relatively rapid decay is seen roughly within 12 ps after excitation. Then the signal shows little decay up to the measured longest time delay beyond 50 ps. At each time delay after excitation, the pump-induced change of the reflected THz electric field $\Delta E(t)$ can be acquired directly by modulating

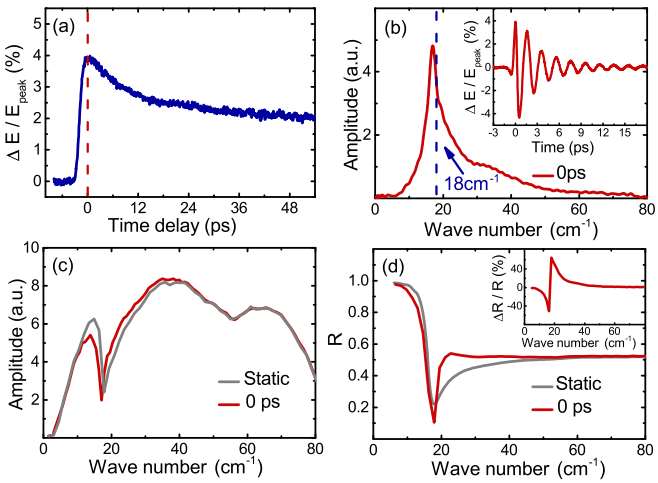

FIG. 2. Pump-induced changes by 1.28-μm excitations at 6 K. (a) The relative electric field change at the THz peak position as a function of time delay after excitation. (b) Inset: The pump-induced relative change $\Delta E(t)/E_{\text{peak}}$ in the time domain at $\tau = 0$ ps. Main panel: The Fourier-transformed spectrum of $\Delta E(t)$. (c) Frequency domain THz spectrum before and after excitation at $\tau = 0$ ps. (d) The reflectivity spectra before and after excitation at $\tau = 0$ ps. The inset shows the ratio of the reflectivity change relative to the static values. The penetration depth mismatch is not considered here.

the pump pulse. Figure 2(b) shows the pump-induced relative change $\Delta E(t)/E_{\text{peak}}$ at 6 K below T_c at $\tau = 0$ ps (inset). $\Delta E(t)/E_{\text{peak}}$ shows clear oscillations in the time domain, which gives a pronounced peak slightly below 18 cm^{-1} in the frequency domain $\Delta E(\omega, \tau)$ after the Fourier transformation, as shown in the main panel of Fig. 2(b). This pronounced peak in $\Delta E(\omega, \tau)$ suggests that the pump-induced change occurs predominantly near the static Josephson plasma edge position. A comparison of the frequency domain THz spectrum after excitation, $E(\omega, \tau) + \Delta E(\omega, \tau)$, with that of the static THz spectrum, $E(\omega, \tau)$, is shown in Fig. 2(c). Obviously, the electric field is reduced below the static plasma edge and enhanced just above the plasma edge for $\tau = 0$ ps.

The complex reflection coefficient of the photoexcited sample $\tilde{r}'(\omega, \tau)$ can be determined from the normalized pump-induced changes to the electric field $\Delta\tilde{E}(\omega, \tau)/\tilde{E}(\omega)$ using the relation $\Delta\tilde{E}(\omega, \tau)/\tilde{E}(\omega) = [\tilde{r}'(\omega, \tau) - \tilde{r}(\omega)]/\tilde{r}(\omega)$, where $\tilde{E}(\omega)$ and $\Delta\tilde{E}(\omega, \tau)$ are obtained from the Fourier transformation of measured $E(t)$ and $\Delta E(t, \tau)$, and the static reflection coefficient $\tilde{r}(\omega)$ is evaluated from the equilibrium optical reflective index obtained from the Kramers-Kronig transformation of optical reflectance measured by FTIR. From $\tilde{r}'(\omega, \tau)$, we can calculate all the optical constants. Figure 2(d) shows the reflectivity spectrum after excitation at $\tau = 0$ ps. The static reflectivity is also plotted for comparison. We find that the reflectivity is suppressed below the static plasma edge and enhanced just above the plasma edge, and merged into the static values roughly above 40 cm^{-1} . Those features can be more clearly seen from the plot of the ratio of reflectivity change over the static values, as shown in the inset of Fig. 2(d).

It deserves to be emphasized that there exists a significant difference in penetration depths between the NIR pump (at 1.28 μm) and the THz probe pulses (below 2.5 THz). To derive the true pump-induced change of THz spectra, the penetration depth mismatch must be taken into account. The data shown above are the raw experimental measurement results of static and pump-induced transient THz spectra at a specific time delay without considering such a mismatch. In the following, we present calculated optical constants from a multilayer model with an incident angle of 30°. Details of the procedure are given in the Supplemental Material [15].

Figure 3 shows the calculated reflectivity, energy loss function, and real part of conductivity spectra at different time delays after 1.28-μm excitations. We first examine the spectral changes at several representative time delays. At the maximum pump-induced signal position, i.e., $\tau = 0$ ps [Fig. 3(a)], the reflectivity below the edge is severely suppressed to low values (roughly below 0.8), though it still displays an edgelike shape. By contrast, the values near the dip position are strongly enhanced and a new heavily overdamped plasma edge appears at a higher energy before merging into the static spectrum. The results suggest that the superconductivity is strongly disturbed or suppressed. However, after a very short time delay, e.g., at $\tau = 1.5$ ps [Fig. 3(b)], a very sharp plasma edge appears at a much lower frequency near 10 cm^{-1}, then a flat reflectance forms, followed by a new broad enhancement with an overdamped edgelike feature at higher energy. With increasing the time delay, e.g., $\tau = 12$ and 54 ps [Figs. 3(c) and 3(d)], the sharp plasma edge at the lower-energy scale shifts to a higher-energy scale, meanwhile, the

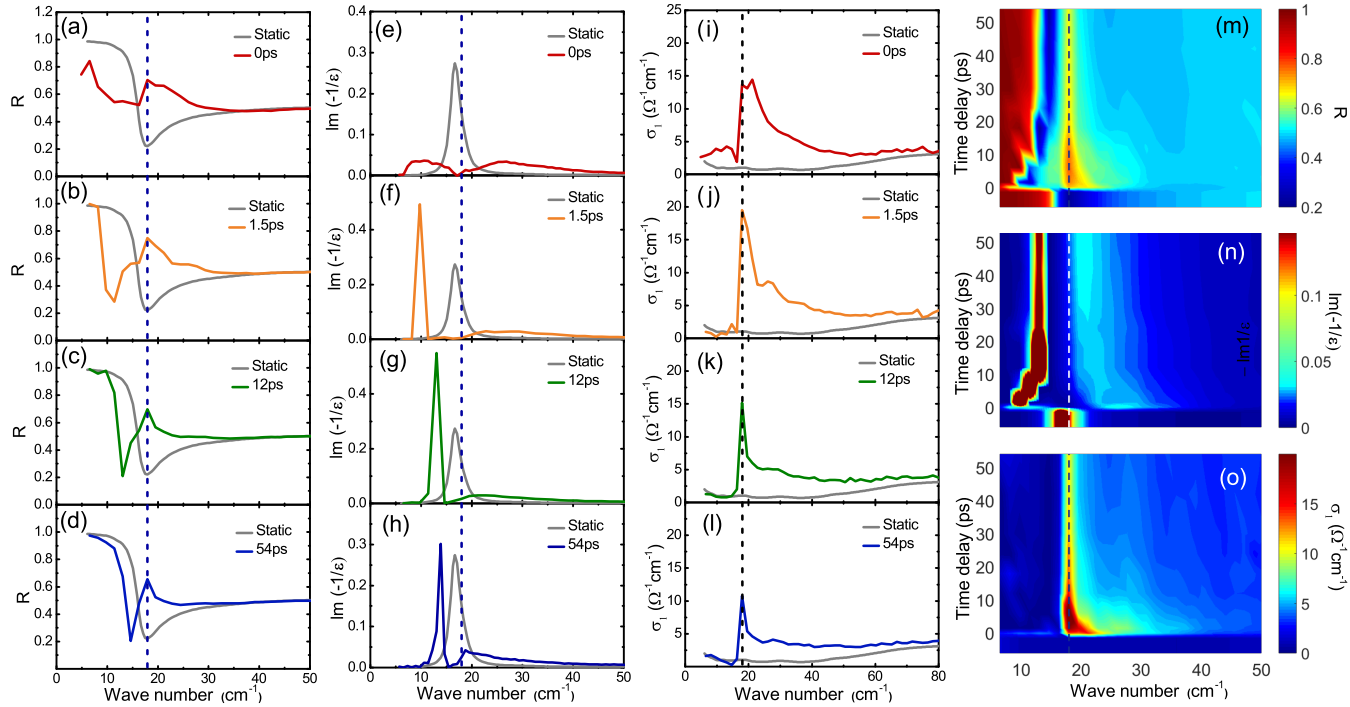

FIG. 3. Calculated optical constants from a multilayer model at different time delays after 1.28-μm excitations. (a)–(d) show the reflectance spectral changes at several representative time delays. (e)–(h) show the corresponding energy loss function spectra. (i)–(l) show the real part of conductivity spectra after excitations. (m)–(o) are intensity plots of the spectral evolution of $R(\omega)$, Im$[-1/\varepsilon(\omega)]$, and $\sigma_1(\omega)$ as a function of time delay.

broad enhancement at high energy weakens and a sharp edge feature appears near 18 cm^{-1} . The observations indicate that the superconductivity is strongly suppressed by the initial photoexcitations, but within a short time delay new Josephson plasmons with different coupling strengths are reestablished. The two edges, which have been well formed after a short time delay of photoexcitations, represent two longitudinal Josephson plasmon modes. They can be identified more clearly as peaks in the energy loss function spectra as presented in Figs. 3(e)–3(h), where the locations of the peaks indicate the energy scales of the mode and their widths reflect the damping rates of the collective excitations. We remark that the splitting of the pump-induced plasma mode was observed in $YBa_2Cu_3O_{6.45}$ with 15-μm excitation [17], however, the signal level was very small and visible only in the differential spectra between the pumped and static spectra. The formation of two extremely strong and long-lived light-induced longitudinal plasmon modes as presented here was not reported before.

The presence of two longitudinal Josephson plasmon modes would lead to the formation of a transverse Josephson plasmon between the two longitudinal modes, which can be regarded as an out-of-phase oscillation of the two individual components [18] and has been observed in many cuprate systems [19–22]. The transverse mode shows up directly in the conductivity spectrum. Indeed, a peak feature is clearly observed in the real part of the conductivity spectra, as presented in Figs. 3(i)–3(l). The peak becomes very sharp and locates at the frequency just slightly lower than the energy of the higher plasmon mode, as indicated in the energy loss function spectra. Besides the narrow peak, a broad enhancement is observed in conductivity above the static Josephson plasmon energy, which is associated with the strongly enhanced reflectivity near and above the static plasma edge energy. This feature is prominent at $\tau = 0$ ps but becomes weaker at longer time delays. This broad feature suggests the development of incoherent quasiparticle excitations with a binding energy above the static plasma edge energy. More detailed spectral evolutions of $R(\omega)$, Im$[-1/\varepsilon(\omega)]$, and $\sigma_1(\omega)$ as a function of time delay are presented in the intensity plots in Figs. 3(m)–3(o), respectively.

We performed similar measurements with MIR excitations at 15 μm. Figure 4(a) shows the decay of the relative change of the THz electric field at the peak position $\Delta E/E_{\text{peak}}$ after excitation at a fluence of 0.5 mJ/cm^2. The decay process is similar to the excitation at 1.28 μm. The pump-induced relative change of $\Delta E(t)/E_{\text{peak}}$ in the time domain and the Fourier-transformed $\Delta E(\omega, \tau)$ in the frequency domain at $T = 6$ K and $\tau = 0$ ps are shown in the inset and main panel of Fig. 4(b), respectively. The shapes are almost the same as that of 1.28-μm excitations, though the signal level is smaller due to a weaker pump fluence. Figures 4(c) and 4(d) show the calculated reflectivity and real part of the conductivity spectra from the multilayer model at two selective time delays $\tau = 0$ and 30 ps and their comparisons with static spectra, respectively. We find that, although the pump-induced spectra are in principle similar to that excited by 1.28 μm shown above, the effect is much smaller. Only a very small peak appears near the static plasma edge position. The high-frequency side edge of the small peak can be assigned to the second longitudinal

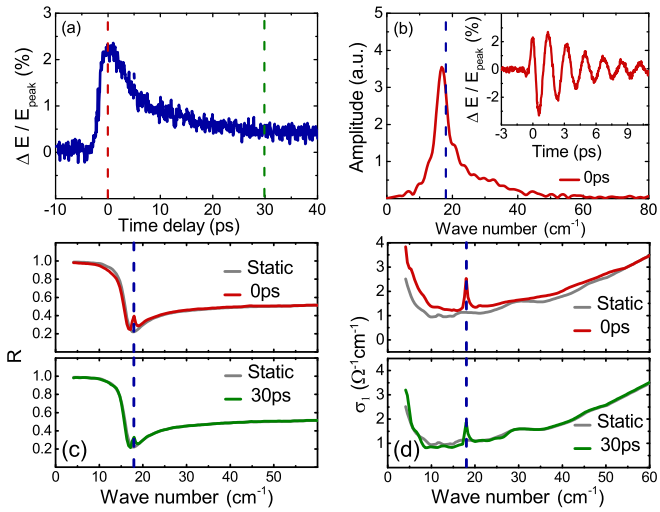

FIG. 4. Pump-induced changes by 15-μm excitations at 6 K. (a) The relative electric field change at the THz peak position as a function of time delay after excitation. (b) The pump-induced relative change of $\Delta E(t)/E_{\text{peak}}$ in the time domain (inset) and the Fourier-transformed $\Delta E(\omega, \tau)$ in the frequency domain (main panel) at $\tau = 0$ ps. (c) and (d) Calculated reflectivity and real part of conductivity from a multilayer model at two time delays $\tau = 0$ and 30 ps and their comparisons with static spectra.

plasmon mode. It leads to a weak feature in the energy loss function (not shown) and a peak in the conductivity spectrum (i.e., transverse plasmon mode). Additionally, the the broad enhancement feature is very weak. The very small effect in the calculated optical constants is attributed to a smaller penetration depth mismatch between the 15-μm and THz probe beam, besides the weaker pump fluence.

We also performed NIR and MIR pump, c-axis terahertz probe measurements at different temperatures. The signal becomes weaker and gradually disappears with increasing temperature. No pump-induced signal is detected above T_c (see Supplemental Material [15]).

We now discuss the implications of the measurement results. An important pump-induced effect is the development of a strong and relatively broad feature in $\sigma_1(\omega)$ at the energy scale above the static plasma edge. It reflects quasiparticle excitations. This feature is prominent with the NIR pump at $\tau = 0$ ps but its intensity decays with time delays. Because it is not Drude-like, we assign it to the incoherent excitations. It implies that the excited quasiparticles are still confined in the ab plane and the c-axis coherence cannot be established due to the insulating block layers. The binding energy has the energy scale of the Josephson coupling strength. Nevertheless, at longer time delays, the reduced spectral weight should become a superconducting condensate centered at zero frequency.

The observation of two long-lived longitudinal Josephson plasmon modes and a transverse plasmon is the most prominent result in this work. It suggests the development of two inequivalent Josephson couplings along the c axis. Its origin is not clear at present. Here, we discuss possible explanations. It is known that the application of a moderate external magnetic field within the CuO_2 plane can have a remarkable effect on the c-axis Josephson plasma mode in underdoped $YBa_2Cu_3O_{7-\delta}$ [23,24]. The applied magnetic field can cause inequivalent insulating layers with and without Josephson vortices, which in turn lead to the modulation formation of Josephson couplings [23,24]. In the present measurement, the electric field of the pump pulse at a fluence of 3 mJ/cm^2 reaches about 6 MV/cm at 1.28-μm pumping. Correspondingly, the magnetic field is about 2 T. The magnetic field at 15-μm pumping is about 0.3 T. The field may be strong enough to generate Josephson vortices in the CuO_2 plane. However, it is unlikely that the ultrafast pulse can generate spatial modulation along the c axis.

One may speculate that the compound locates not far from the charge stripe phase in the phase diagram, and a dynamical stripe fluctuation may exist in the sample. Since the charge stripes, whose directions change by 90° in the neighboring CuO_2 planes, can lead to spatial modulation of the Josephson coupling strengths between the superconducting charge stripes [25,26], the observation of two longitudinal plasma edges may be related to the dynamical stripes. We think that this possibility is low since the compound exhibits a single and very sharp Josephson plasma edge without pumping. The intense pumping is unlikely to induce the formation of charge stripe order. In fact, a recent time-resolved resonant soft x-ray diffraction study indicated that the NIR excitations suppress the stripe order in the $La_{1.885}Ba_{0.115}CuO_4$ sample [27].

A more plausible explanation is that strong photoexcitations induce a structural change in the compound. If the intense pump pulse can drive the out-of-plane apical oxygens to deviate their equilibrium positions, resulting in a modulation of Cu-apical oxygen bond lengths between different CuO_2 planes, two different Josephson coupling strengths can naturally develop. This would explain the formation of two longitudinal Josephson plasmons and a transverse mode. In fact, photoinduced structural phase transitions have been found in different compounds [28–31]. For example, a photoinduced homogeneous, metastable lattice change was observed in $Nd_{0.5}Sr_{0.5}MnO_3$ using time-resolved x-ray diffraction [31]. An earlier ultrafast electron diffraction measurement on $La_2CuO_{4+\delta}$ actually indicated a photoinduced structural change with an increase of the c-axis lattice constant [30]. Nevertheless, further detailed studies on the photoinduced structural change and its decay dynamics by other time-resolved probes below T_c are needed to test this scenario.

To summarize, we performed NIR and MIR pump, c-axis THz probe measurements on a superconducting single crystal $La_{1.905}Ba_{0.095}CuO_4$ with $T_c = 32$ K. The measurement reveals that the pump-induced change occurs mainly at the Josephson plasma edge position below T_c. The superconducting state is severely disturbed by the strong NIR excitations and incoherent quasiparticle excitations develop in the frequency regime above the static plasma edge. Most prominently, we observe the reappearance of a very sharp Josephson plasma edge at a frequency lower than the static Josephson plasma edge and a new light-induced Josephson mode at a higher energy after a short time delay. The results imply that light can induce new Josephson plasmons with different coupling strengths. A similar but weak effect is observed for the MIR pump.

We acknowledge very useful discussions with Shin-ichi Uchida, Setsuko Tajima, and John Tranquada. This work was supported by the National Science Foundation of China (No. 11327806 and No. GZ1123) and the National Key Research and Development Program of China (No.2016YFA0300902 and No. 2017YFA0302904).

S.J.Z. and Z.X.W. contributed equally to this work.

[1] M. Rini, R. Tobey, N. Dean, J. Itatani, Y. Tomioka, Y. Tokura, R. W. Schoenlein, and A. Cavalleri, Nature (London) **449**, 72 (2007).

[2] K. W. Kim, A. Pashkin, H. Schäfer, M. Beyer, M. Porer, T. Wolf, C. Bernhard, J. Demsar, R. Huber, and A. Leitenstorfer, Nat. Mater. **11**, 497 (2012).

[3] M. Porer, U. Leierseder, J.-M. Ménard, H. Dachraoui, L. Mouchliadis, I. E. Perakis, U. Heinzmann, J. Demsar, K. Rossnagel, and R. Huber, Nat. Mater. **13**, 857 (2014).

[4] L. Stojchevska, I. Vaskivskyi, T. Mertelj, P. Kusar, D. Svetin, S. Brazovskii, and D. Mihailovic, Science **344**, 177 (2014).

[5] R. Matsunaga, Y. I. Hamada, K. Makise, Y. Uzawa, H. Terai, Z. Wang, and R. Shimano, Phys. Rev. Lett. **111**, 057002 (2013).

[6] R. Y. Chen, S. J. Zhang, M. Y. Zhang, T. Dong, and N. L. Wang, Phys. Rev. Lett. **118**, 107402 (2017).

[7] T. Arikawa, K. Hyodo, Y. Kadoya, and K. Tanaka, Nat. Phys. **13**, 688 (2017).

[8] D. Fausti, R. I. Tobey, N. Dean, S. Kaiser, A. Dienst, M. C. Hoffmann, S. Pyon, T. Takayama, H. Takagi, and A. Cavalleri, Science **331**, 189 (2011).

[9] S. Kaiser, C. R. Hunt, D. Nicoletti, W. Hu, I. Gierz, H. Y. Liu, M. Le Tacon, T. Loew, D. Haug, B. Keimer, and A. Cavalleri, Phys. Rev. B **89**, 184516 (2014).

[10] W. Hu, S. Kaiser, D. Nicoletti, C. R. Hunt, I. Gierz, M. C. Hoffmann, M. Le Tacon, T. Loew, B. Keimer, and A. Cavalleri, Nat. Mater. **13**, 705 (2014).

[11] D. Nicoletti, E. Casandruc, Y. Laplace, V. Khanna, C. R. Hunt, S. Kaiser, S. S. Dhesi, G. D. Gu, J. P. Hill, and A. Cavalleri, Phys. Rev. B **90**, 100503(R) (2014).

[12] E. Casandruc, D. Nicoletti, S. Rajasekaran, Y. Laplace, V. Khanna, G. D. Gu, J. P. Hill, and A. Cavalleri, Phys. Rev. B **91**, 174502 (2015).

[13] M. Hücker, M. v. Zimmermann, G. D. Gu, Z. J. Xu, J. S. Wen, G. Xu, H. J. Kang, A. Zheludev, and J. M. Tranquada, Phys. Rev. B **83**, 104506 (2011).

[14] S. J. Zhang, Z. X. Wang, T. Dong, and N. L. Wang, Front. Phys. **12**, 127802 (2017).

[15] See Supplemental Material at http://link.aps.org/supplemental/10.1103/PhysRevB.98.020506 for details of the experimental setup and the procedure to calculate the light-induced transient optical constants using multilayer and single layer models.

[16] C. C. Homes, M. Hücker, Q. Li, Z. J. Xu, J. S. Wen, G. D. Gu, and J. M. Tranquada, Phys. Rev. B **85**, 134510 (2012).

[17] C. R. Hunt, D. Nicoletti, S. Kaiser, D. Pröpper, T. Loew, J. Porras, B. Keimer, and A. Cavalleri, Phys. Rev. B **94**, 224303 (2016).

[18] D. van der Marel and A. Tsvetkov, Czech. J. Phys. **46**, 3165 (1996).

[19] H. Shibata and T. Yamada, Phys. Rev. Lett. **81**, 3519 (1998).

[20] M. Grueninger, D. van der Marel, A. A. Tsvetkov, and A. Erb, Phys. Rev. Lett. **84**, 1575 (1999).

[21] T. Timusk and C. C. Homes, Solid State Commun. **126**, 63 (2003).

[22] S. Tajima and S. I. Uchida, Physica C (Amsterdam) **481**, 55 (2012).

[23] K. M. Kojima, S. Uchida, Y. Fudamoto, and S. Tajima, Phys. Rev. Lett. **89**, 247001 (2002).

[24] A. D. LaForge, W. J. Padilla, K. S. Burch, Z. Q. Li, S. V. Dordevic, K. Segawa, Y. Ando, and D. N. Basov, Phys. Rev. B **76**, 054524 (2007).

[25] B. P. Gorshunov, A. A. Voronkov, V. S. Nozdrin, E. S. Zhukova, T. Matsuoka, K. Tanaka, S. Miyasaka, S. Tajima, and M. Dressel, Solid State Commun. **151**, 1681 (2011).

[26] A. A. Voronkov, B. P. Gorshunov, V. S. Nozdrin, E. S. Zhukova, T. Matsuoka, K. Tanaka, S. Miyasaka, S. Tajima, and M. Dressel, JETP Lett. **94**, 708 (2012).

[27] V. Khanna, R. Mankowsky, M. Petrich, H. Bromberger, S. A. Cavill, E. Mohr-Vorobeva, D. Nicoletti, Y. Laplace, G. D. Gu, J. P. Hill, M. Forst, A. Cavalleri, and S. S. Dhesi, Phys. Rev. B **93**, 224522 (2016).

[28] A. Cavalleri, C. Tóth, C. W. Siders, J. A. Squier, F. Ráksi, P. Forget, and J. C. Kieffer, Phys. Rev. Lett. **87**, 237401 (2001).

[29] B. J. S. Vance R. Morrison, R. P. Chatelain, K. L. Tiwari, A. Hendaoui, A. Bruhács, and M. Chaker, Science **346**, 445 (2014).

[30] N. Gedik, D.-s. Yang, G. Logvenov, I. Bozovic, and A. H. Zewail, Science **316**, 425 (2007).

[31] H. Ichikawa, S. Nozawa, T. Sato, A. Tomita, K. Ichiyanagi, M. Chollet, L. Guerin, N. Dean, A. Cavalleri, S.-I. Adachi, T.-H. Arima, H. Sawa, Y. Ogimoto, M. Nakamura, R. Tamaki, K. Miyano, and S.-y. Koshihara, Nat. Mater. **10**, 101 (2011).